Optica Applicata, Vol. LV, No. 4, 2025
DOI: 10.37190/oa/209624

Focusing characteristics of Bessel–Gaussian vortex beams with heterogeneous phase modulation

HAO WANG[1], JINSONG LI[1,*], CHUNDI ZHENG[2,*]

[1] China Jiliang University, College of Optics and Electronic, Hangzhou 310018, P.R. China

[2] National Institute of Metrology, Beijing 10029, P.R. China

[*]Corresponding authors: lijinsong@cjlu.edu.cn (J.L.), zhengchundi@nim.ac.cn (C.Z.)

Using vector diffraction theory, we analyze how heterogeneous phase modulation affects the focusing behavior and propagation of Bessel–Gaussian beams. We systematically analyze the influence of beam parameters, topological charge L, phase factor n, and focusing angle phase parameter B on the normalized intensity distribution. The results reveal that the topological charge L can precisely control the opening degree of the spiral-shaped curve on the focal plane: as L increases, the ring opening widens, and a second ring emerges. Increasing the phase factor n concentrates beam energy toward the central spot. The focusing angle phase parameter B strongly affects peak intensity locations: larger B shifts energy toward bilateral regions, and further increase displaces the highest -intensity spot outward along the $y = x$ direction. Increasing beam parameters causes focal plane intensity peaks to separate, expanding the overall focal pattern outward. We also examine how negative B values alter peak intensity positions. As B decreases, peak intensity locations rotate clockwise. These findings have potential applications in optical trapping, particle manipulation, and modern medical technologies.

Keywords: focusing characteristics, heterogeneous phase, vector diffraction theory, Bessel–Gaussian vortex beams.

1. Introduction

In 1987, James Durnin first proposed the concept of an ideal Bessel beam, which exhibits a diffraction-free property. Its transverse intensity profile is described by a Bessel function and theoretically maintains its shape over an infinite propagation distance. However, such ideal Bessel beams require infinite energy, making them experimentally unrealizable [1,2].

To overcome this limitation, GORI *et al*. introduced the Bessel–Gaussian beam model, which multiplies a Bessel function with a Gaussian envelope. This modification eliminates the infinite energy requirement, providing a practical approximation of diffraction-free beams [3].

In the 1990s, researchers successfully generated Bessel–Gaussian beams experimentally using axicons, annular apertures combined with lens systems, or laser mode converters. These methods achieved the desired Bessel–Gaussian intensity profile by modulating the laser wavefront phase [4,5].

In recent decades, research has expanded beyond beam propagation to include tight -focusing systems, leading to widespread applications of tightly focused Bessel–Gaussian beams with high numerical aperture objectives [6-11]. For example, LIU *et al*. demonstrated that radially polarized Bessel–Gaussian vortex beams with a power-exponent phase profile produce subwavelength focal spots with strong longitudinal fields under high-NA focusing. Such configurations show potential for optical trapping of multiple particles and laser fabrication of chiral microstructures [12].

However, studies on Bessel–Gaussian beams with heterogeneous phase modulation remain relatively scarce [13]. In practice, many optical applications, such as light field manipulation or optical devices, deliberately employ spatially or temporally nonuniform phase distributions. Unlike uniform phase distributions, heterogeneous phase structures break symmetry and introduce controlled wavefront propagation differences, enabling unprecedented manipulation of optical amplitude, polarization, and momentum. Metasurfaces leverage spatially varying phase profiles to achieve light deflection [14-16], orbital angular momentum beam generation [17-19], or sub-diffraction-limit focusing [20-23]. This motivates our further investigation into how heterogeneous phase modulation influences beam focusing.

2. Theory

This study focuses on the focusing properties of Bessel–Gaussian vortex beams with heterogeneous phase modulation. The scheme of the optical system is shown in Fig. 1.

The heterogeneous phase function can be expressed as:

$$\exp(iB\,\mathrm{NA}^{-1}\sin\theta + iL\varphi)\exp\left[i\pi\sin(n\varphi) + i\pi\cos(n\varphi)\right] \tag{1}$$

Here, B is the focusing angle phase parameter, n is the phase factor parameter, L is the topological charge of the helical phase component, and NA is the numerical aperture of the focusing system. J_0 denotes the zero-order Bessel function, β represents the

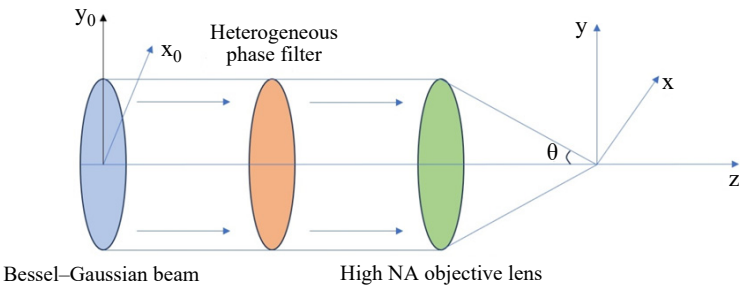

Fig. 1. System structure diagram.

beam parameter, and ω is the waist width of the Bessel–Gauss beam. Thus, a vortex beam with heterogeneous phase modulation in a focused optical system can be expressed as follows [24]:

$$E(r,\varphi) = J_0\left(\frac{\beta(r/a)^2}{(\omega/a)^2}\right)\exp\left(-\frac{(r/a)^2}{(\omega/a)^2}\right) \times \exp(iB\,\mathrm{NA}^{-1}\sin\theta + iL\varphi) \times \exp\left[i\pi\sin(n\varphi) + i\pi\cos(n\varphi)\right] \tag{2}$$

In cylindrical coordinates denoted as $r = f\sin\theta$, where $a = f\sin\theta_{\max}$, substitution into the above equation yields:

$$E(\theta,\varphi) = J_0\left(\frac{\beta(f\sin\theta/f\sin\theta_{\max})^2}{(\omega/a)^2}\right)\exp\left(-\frac{(f\sin\theta/f\sin\theta_{\max})^2}{(\omega/a)^2}\right) \times \exp(iB\,\mathrm{NA}^{-1}\sin\theta + iL\varphi) \times \exp\left[i\pi\sin(n\varphi) + i\pi\cos(n\varphi)\right] \tag{3}$$

Assuming the system is in air, where $\theta \in [0, \arcsin(\mathrm{NA})]$ and $\mathrm{NA} = \sin\theta_{\max}$, the above equation can be further modified to:

$$E(\theta,\varphi) = J_0\left(\frac{\beta\sin^2\theta}{\mathrm{NA}^2(\omega/a)^2}\right)\exp\left(-\frac{\sin^2\theta}{\mathrm{NA}^2(\omega/a)^2}\right) \times \exp(iB\,\mathrm{NA}^{-1}\sin\theta + iL\varphi) \times \exp\left[i\pi\sin(n\varphi) + i\pi\cos(n\varphi)\right] \tag{4}$$

When the incident light is polarized along the x-axis, the electric field distribution in the focal region can be derived using Richards–Wolf vector diffraction theory as [25,26]:

$$\mathbf{E}(\rho,\psi,z) = \frac{1}{\lambda}\iint_{\Omega} E(\theta,\varphi)\begin{Bmatrix}[\cos\theta + \sin^2\varphi(1-\cos\theta)]\mathbf{x}\\ \cos\varphi\sin\varphi(\cos\theta - 1)\mathbf{y}\\ \cos\varphi\sin\theta\,\mathbf{z}\end{Bmatrix} \times \exp\left[-ik\rho\sin\theta\cos(\varphi-\psi)\right]\exp(-ikz\cos\theta)\sin\theta\,\mathrm{d}\theta\,\mathrm{d}\varphi \tag{5}$$

where ρ, ψ, z are cylindrical coordinates in the focal region, **x**, **y**, **z** are Cartesian unit vectors, and $k = 2\pi/\lambda$ is the wave number.

Substituting Eq. (4) into Eq. (5) yields the electric field within the focal region along the x, y, and z directions.

The electric field in the x direction is

$$\begin{aligned}\mathbf{E}_x(\rho, \psi, z) = \frac{A}{\lambda}\int_0^{\theta_{\max}}\int_0^{2\pi} J_0\left(\frac{\beta\sin^2\theta}{\mathrm{NA}^2(\omega/a)^2}\right)\exp\left(-\frac{\sin^2\theta}{\mathrm{NA}^2(\omega/a)^2}\right)\\ \times \exp(iB\,\mathrm{NA}^{-1}\sin\theta + iL\varphi)\exp\left[i\pi\sin(n\varphi) + i\pi\cos(n\varphi)\right]\\ \times \left[\cos\theta + \sin^2\varphi(1-\cos\theta)\right]\exp\left[-ik\rho\sin\theta\cos(\varphi-\psi)\right]\\ \times \exp(-ikz\cos\theta)\sin\theta\,\mathrm{d}\theta\,\mathrm{d}\varphi \qquad (6)\end{aligned}$$

the electric field in the y direction is

$$\begin{aligned}\mathbf{E}_y(\rho, \psi, z) = \frac{A}{\lambda}\int_0^{\theta_{\max}}\int_0^{2\pi} J_0\left(\frac{\beta\sin^2\theta}{\mathrm{NA}^2(\omega/a)^2}\right)\exp\left(-\frac{\sin^2\theta}{\mathrm{NA}^2(\omega/a)^2}\right)\\ \times \exp(iB\,\mathrm{NA}^{-1}\sin\theta + iL\varphi)\exp\left[i\pi\sin(n\varphi) + i\pi\cos(n\varphi)\right]\\ \times \cos\varphi\sin\varphi(\cos\theta - 1)\exp\left[-ik\rho\sin\theta\cos(\varphi-\psi)\right]\\ \times \exp(-ikz\cos\theta)\sin\theta\,\mathrm{d}\theta\,\mathrm{d}\varphi \qquad (7)\end{aligned}$$

and the electric field in the z direction is

$$\begin{aligned}\mathbf{E}_z(\rho, \psi, z) = \frac{A}{\lambda}\int_0^{\theta_{\max}}\int_0^{2\pi} J_0\left(\frac{\beta\sin^2\theta}{\mathrm{NA}^2(\omega/a)^2}\right)\exp\left(-\frac{\sin^2\theta}{\mathrm{NA}^2(\omega/a)^2}\right)\\ \times \exp(iB\,\mathrm{NA}^{-1}\sin\theta + iL\varphi)\exp\left[i\pi\sin(n\varphi) + i\pi\cos(n\varphi)\right]\\ \times \cos\varphi\sin\theta\exp\left[-ik\rho\sin\theta\cos(\varphi-\psi)\right]\\ \times \exp(-ikz\cos\theta)\sin\theta\,\mathrm{d}\theta\,\mathrm{d}\varphi \qquad (8)\end{aligned}$$

3. Numerical results

Building upon the equations derived in the preceding section, we perform numerical simulations to analyze the optical field distribution and examine the properties of

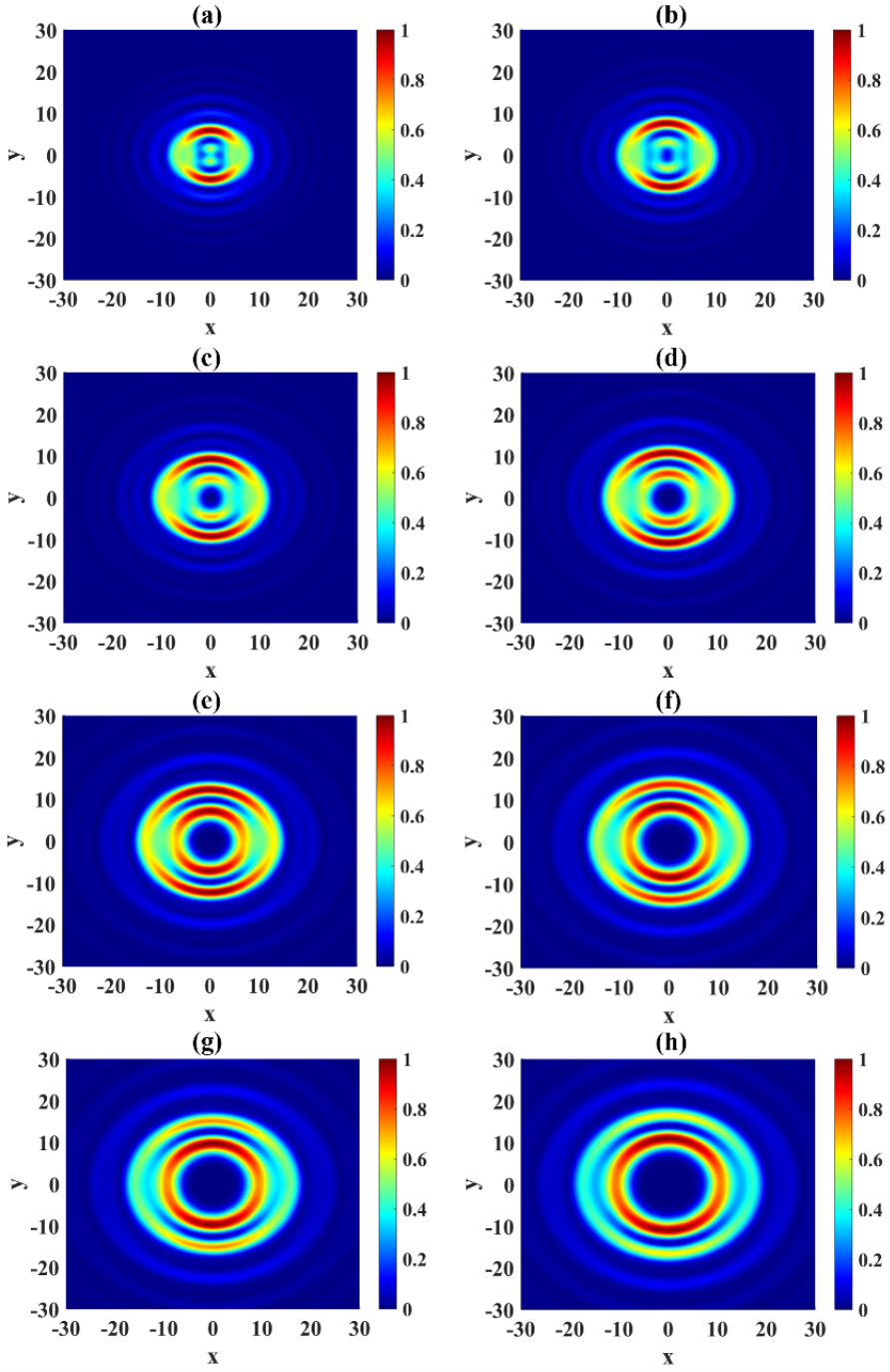

Fig. 2. Intensity distribution of the focused field for a Bessel–Gaussian beam with heterogeneous phase modulation under the following conditions: NA = 0.95, $n = 0$, $B = 1$, $\beta = 5$, and (a) $L = 1$, (b) $L = 2$, (c) $L = 3$, (d) $L = 4$, (e) $L = 5$, (f) $L = 6$, (g) $L = 7$, and (h) $L = 8$.

Bessel–Gaussian beams under heterogeneous phase modulation. For our analysis, we assume a focusing optical system with numerical aperture NA = 0.95 and relative beam waist width $\omega = 1$, without compromising the validity or generality of our results. All distance units in the figures are normalized to k^{-1}, where k denotes the wave number.

Figure 2 presents the intensity distributions at the focal plane for varying topological charges L, with the system parameters set as NA = 0.95, $n = 0$, $B = 1$, and $\beta = 5$. When $L = 1$, the intensity distribution on the focal plane appears as a symmetric circular ring, as illustrated in Fig. 2(a). As the value of L increases, the intensity distribution gradually expands, and the diameter of the circular ring also enlarges. At $L = 4$, compared to $L = 1$, a second ring emerges within the circular intensity pattern. With further increases in the topological charge L, the second ring progressively approaches a uniform circular intensity distribution. From Fig. 2(a) to (h), it can be concluded that the topological charge L significantly influences the intensity distribution in the focal region: the overall intensity distribution expands outward, and as L increases, the intensity of the first ring decreases while the intensity of the second ring increases. Moreover, the intensity distribution of the second ring becomes more uniform compared to the first.

Investigating the influence of the focusing angle phase parameter B on beam intensity distribution, Fig. 3 presents and analyzes the intensity distribution of Bessel–Gauss beams with heterogeneous phase modulation under the conditions of numerical aperture NA = 0.95, $L = 1$, $B = 5$, and $\beta = 5$. The simulation results reveal that the intensity distribution undergoes significant changes as the focusing angle phase parameter B varies. When $n = 0.1$, two intensity bright spots appear symmetrically along the vertical axis, with the upper spot exhibiting higher intensity than the lower one. As n increases to 0.4, the upper and lower bright spots gradually merge, forming a single high-intensity spot. When n further rises to 0.8, the focal plane stabilizes into a steady intensity distribution, maintaining a single well-defined bright spot. These observations demonstrate that the focusing angle phase parameter B effectively modulates the energy distribution of the intensity pattern, and compared with the previous research results [24], the focus of the beam can be controlled more sensitively by adjusting focusing angle phase parameter B.

To study the influence of different beam parameters β on the intensity distribution at the focal plane, we simulated the intensity profiles of Bessel–Gauss beams with heterogeneous phase modulation under the conditions of numerical aperture NA = 0.95, $L = 1$, $n = 1$, and $B = 1$, as shown in Fig. 4. When the beam parameter $\beta = 2$, two intensity peaks appear near the geometric focus. As β increases to 9, the overall focal pattern expands (Fig. 4(c)). With further increases in β, the separation between the two intensity peaks gradually widens (Figs. 4(e) to (h)). Additionally, the upper intensity peak shifts upward, while the central peak moves from the focal center toward the right.

Under the conditions of numerical aperture NA = 0.95, $n = 2$, $\beta = 1$, and topological charge $L = 1$, Fig. 5 presents the focal-plane intensity distributions of Bessel–Gauss beams with heterogeneous phase modulation for different focusing angle phase parameter B. As shown in Fig. 5(a), the focal pattern exhibits central symmetry. When B in-

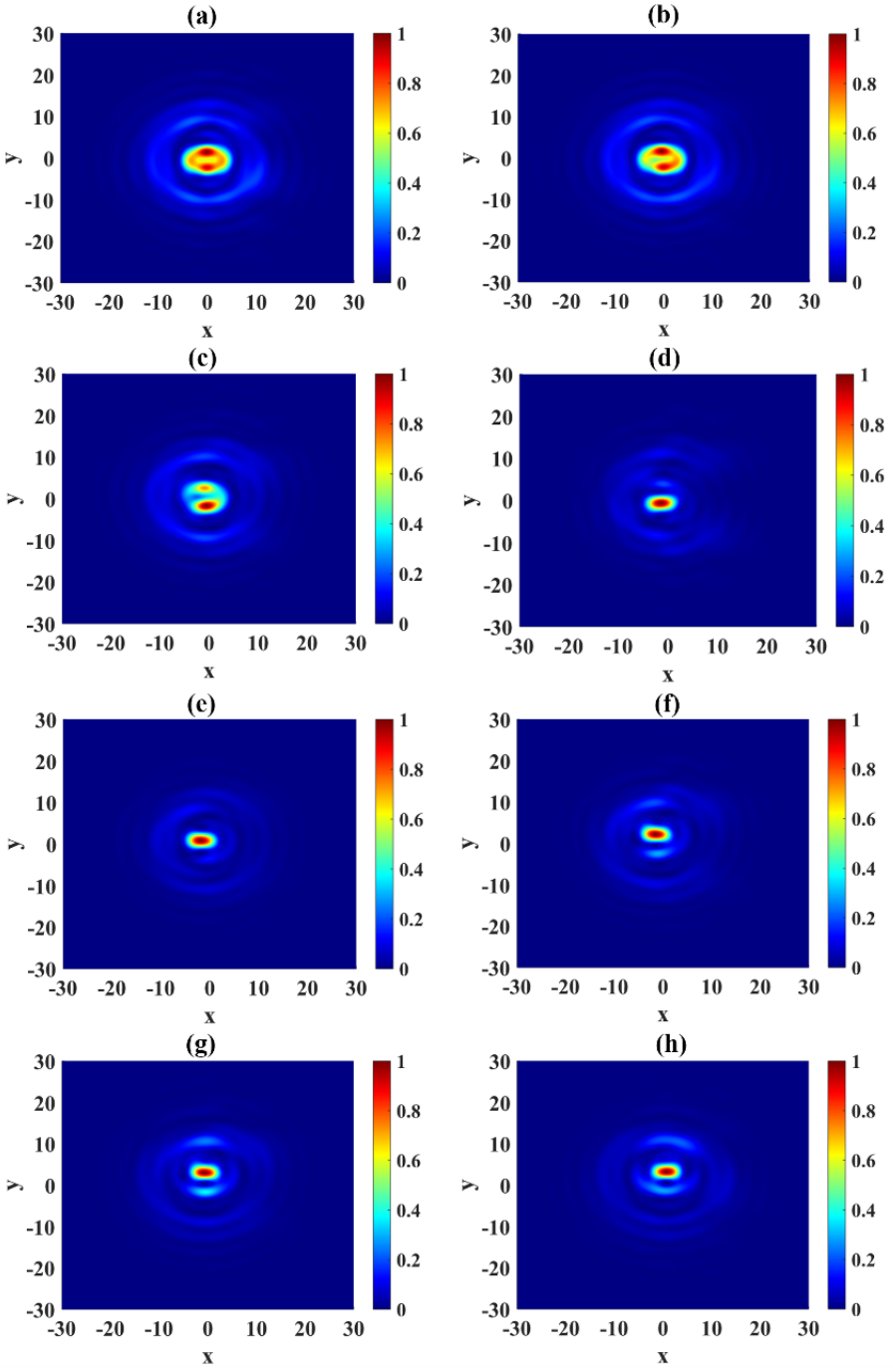

Fig. 3. Intensity distribution of the focused field for a Bessel–Gaussian beam with heterogeneous phase modulation under the following conditions: NA = 0.95, $L = 1$, $B = 5$, $\beta = 5$, and (a) $n = 0.1$, (b) $n = 0.2$, (c) $n = 0.3$, (d) $n = 0.4$, (e) $n = 0.5$, (f) $n = 0.6$, (g) $n = 0.7$, and (h) $n = 0.8$.

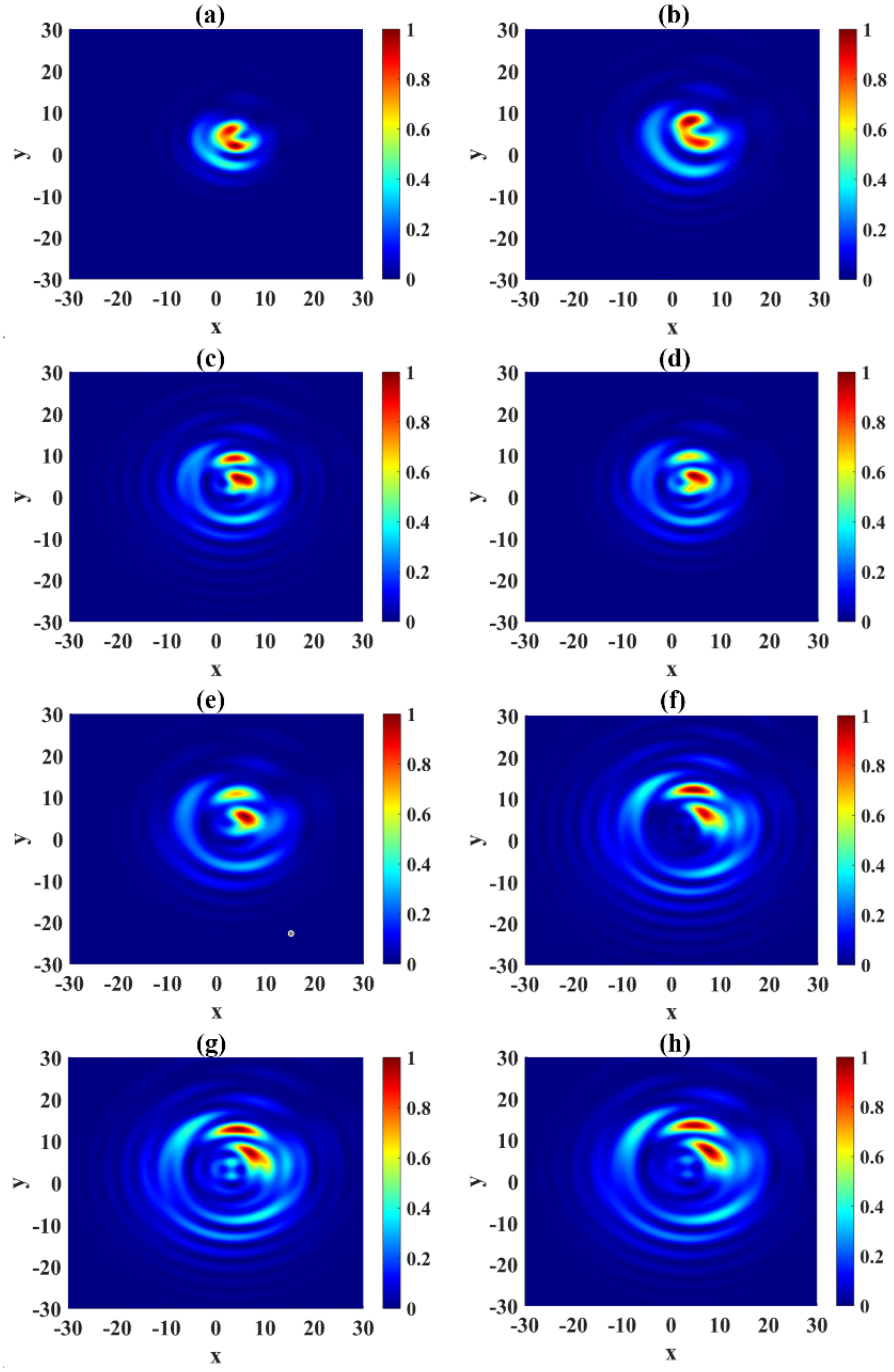

Fig. 4. Intensity distribution of the focused field for a Bessel–Gaussian beam with heterogeneous phase modulation under the following conditions: NA = 0.95, $L = 1$, $B = 1$, $n = 1$, and (a) $\beta = 2$, (b) $\beta = 3$, (c) $\beta = 4$, (d) $\beta = 5$, (e) $\beta = 6$, (f) $\beta = 7$, (g) $\beta = 8$, and (h) $\beta = 9$.

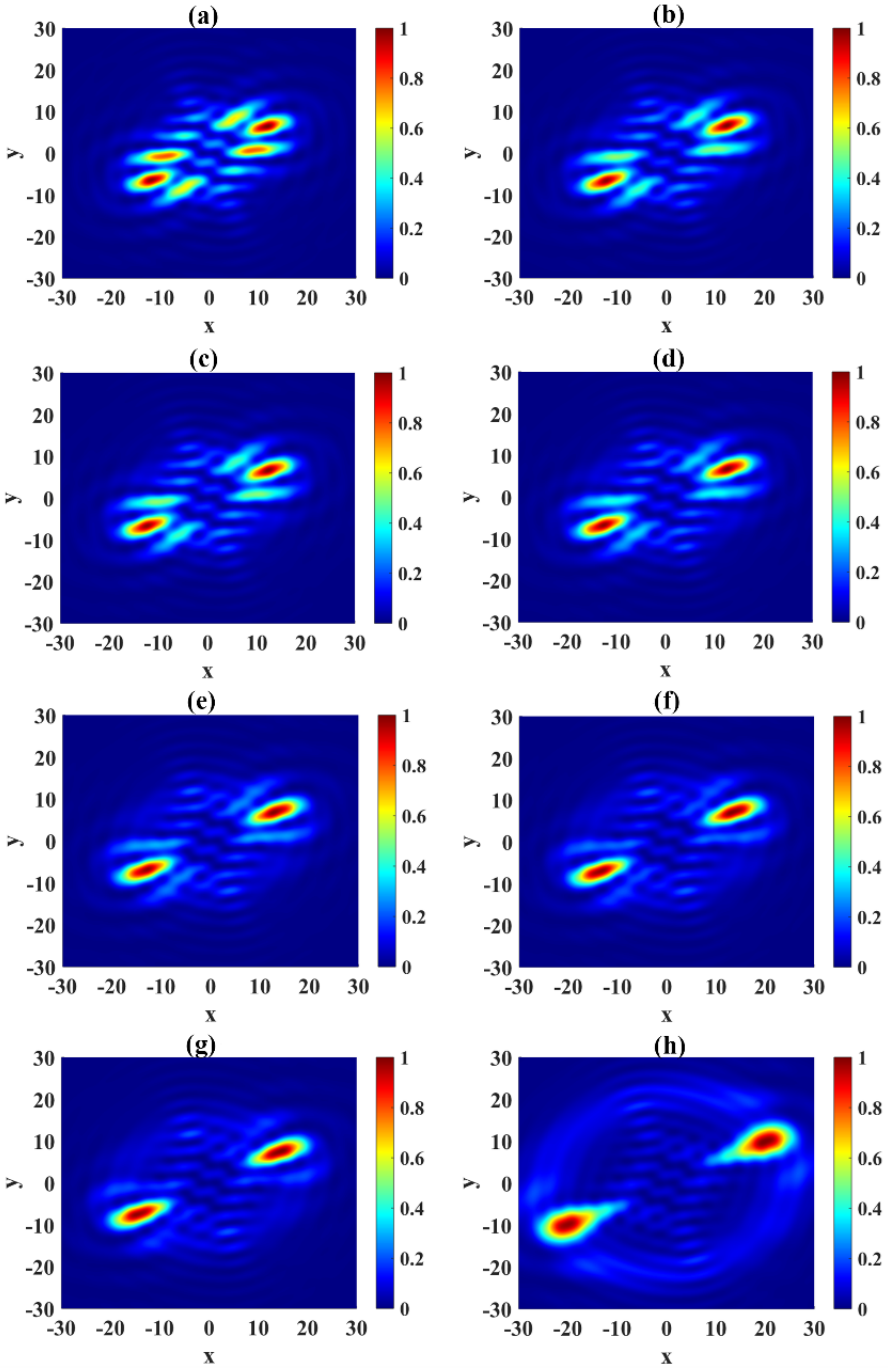

Fig. 5. Intensity distribution of the focused field for a Bessel–Gaussian beam with heterogeneous phase modulation under the following conditions: NA = 0.95, $L = 1$, $\beta = 1$, $n = 2$, and (a) $B = 7$, (b) $B = 8$, (c) $B = 9$, (d) $B = 10$, (e) $B = 11$, (f) $B = 12$, (g) $B = 13$, and (h) $B = 20$.

creases from 7 to 11, the intensity distribution gradually concentrates toward both sides, evolving from multiple discrete spots into two large, symmetrically positioned intensity lobes. With further increase of B to 20, the intensity distribution continues to expand, and the intensity peaks are observed to shift slowly along the diagonal direction. This demonstrates that the dimensionless axicon parameter B effectively controls both the spatial concentration and directional movement of the focal intensity distribution. Therefore, by adjusting focusing angle phase parameter B, two particles can be separated along a certain trajectory.

Under the parameters NA = 0.95, $L = -1$, $\beta = 1$, and $n = 0.8$, the focal light intensity distribution varies with parameter B, as illustrated in Fig. 6. When the focusing angle

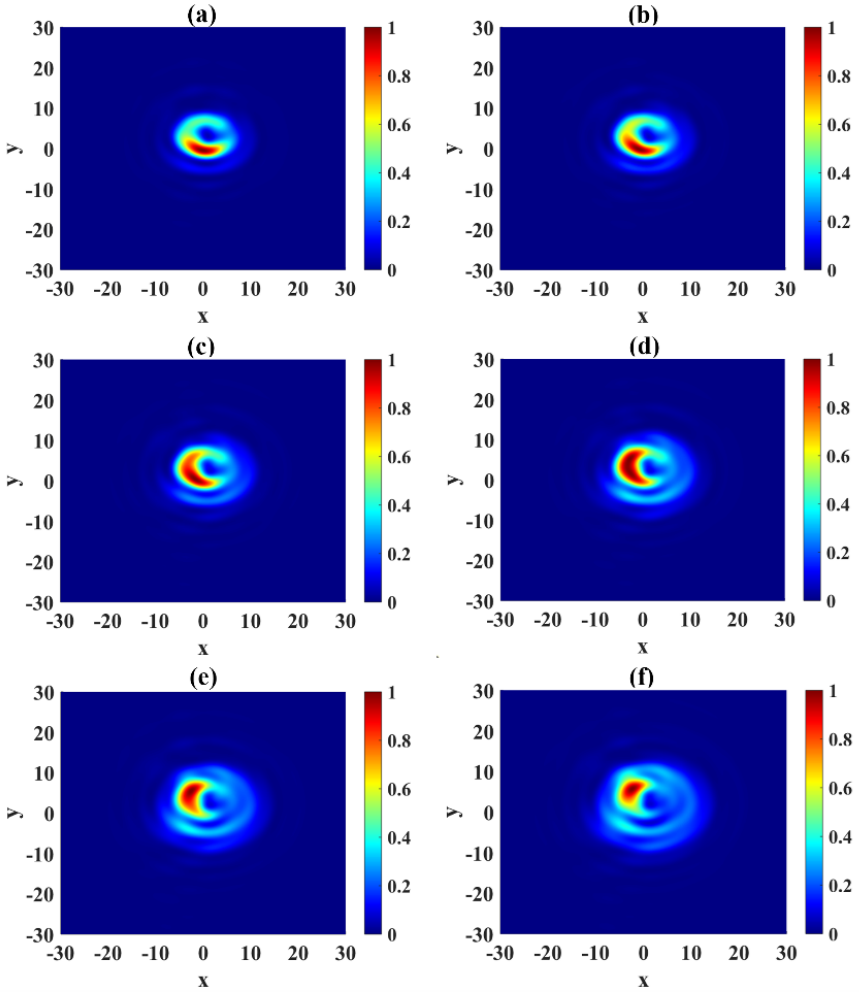

Fig. 6. Intensity distribution of the focused field for a Bessel–Gaussian beam with heterogeneous phase modulation under the following conditions: NA = 0.95, $L = -1$, $\beta = 1$, $n = 0.8$, and (a) $B = -1$, (b) $B = -2$, (c) $B = -3$, (d) $B = -4$, (e) $B = -5$, and (f) $B = -6$.

phase parameter $B = -1$, the peak intensity is located directly beneath the circular focal pattern. As B decreases to –2, the peak intensity within the focal pattern rotates. As shown in Figs. 6(e) and (f), further reduction in B shifts the peak intensity toward the upper-left corner, while the focal spot gradually expands. By regulating focusing angle phase parameter B, it can be used for the rotation of particles.

4. Conclusions

We investigated the focusing and propagation properties of Bessel–Gaussian beams with heterogeneous phase modulation, systematically analyzing the influence of key parameters beam parameter β, topological charge L, phase factor n, and focusing angle phase parameter B on the normalized intensity distribution. Our findings demonstrate that: Topological charge L precisely controls the focal ring's aperture size, with increasing L leading to a more pronounced ring opening and the emergence of a secondary ring. Phase factor n drives beam energy concentration toward the central spot, offering tunability for applications requiring high-intensity focal spots. Focusing angle phase parameter B critically determines the position of intensity peaks: Positive B causes energy concentration on both sides, with peak locations shifting outward along $y = x$ as B increases. Negative B induces a clockwise rotation of peak intensity positions with decreasing B. Beam parameter β governs focal region expansion, with larger β values leading to outward separation of intensity maxima. These variations in intensity distribution, achievable through parameter adjustments, open new avenues for optical applications. Specifically: by adjusting focusing angle phase parameter B, two particles can be separated along a certain trajectory. By regulating focusing angle phase parameter B, it can be used for the rotation of particles. These findings provide new perspectives on particle transfer and transport, optical shaping, particle capture, and optical micromanipulation.

Acknowledgements
This work is supported by the National Key R&D Projects, China (2021YFF0600204).

Data availability
Data underlying the results presented in this paper are not publicly available at this time but may be obtained from the authors upon reasonable request.

Declarations
Conflict of interest The authors declare no conflicts of interest.

References

[1] Durnin J., *Exact solutions for nondiffracting beams. I. The scalar theory*, Journal of the Optical Society of America A **4**(4), 1987: 651-654. https://doi.org/10.1364/JOSAA.4.000651

[2] Durnin J., Miceli J.J., Eberly J.H., *Diffraction-free beams*, Physical Review Letters **58**(15), 1987: 1499-1501.

[3] Gori F., Guattari G., Padovani C., *Bessel-Gauss beams*, Optics Communications **64**(6), 1987: 491 -495. https://doi.org/10.1016/0030-4018(87)90276-8

[4] VASARA A., TURUNEN J., FRIBERG A.T., *Realization of general nondiffracting beams with computer -generated holograms*, Journal of the Optical Society of America A **6**(11), 1989: 1748-1754. https://doi.org/10.1364/JOSAA.6.001748
[5] HERMAN R.M., WIGGINS T.A., *Production and uses of diffractionless beams*, Journal of the Optical Society of America A **8**(6), 1991: 932-942. https://doi.org/10.1364/JOSAA.8.000932
[6] LUKIN I.P., *Integral momenta of vortex Bessel-Gaussian beams in turbulent atmosphere*, Applied Optics **55**(12), 2016: B61-B66. https://doi.org/10.1364/AO.55.000B61
[7] ZHAN Q., ZHANG R., DING S., WANG G., GAO X., *Focusing pattern of axisymmetric Bessel–Gaussian beam with helical polarization under triangular modulation*, Applied Optics **59**(3), 2020: 648-652. https://doi.org/10.1364/AO.376445
[8] LI J., GAO X., ZHANG S., ZHUANG S., *Focusing properties of Gaussian beam with mixed screw and conical phase fronts*, Optik **121**(19), 2010: 1794-1798. https://doi.org/10.1016/j.ijleo.2009.04.016
[9] DONG X., GENG T., ZHUANG S., *Focus shaping of Weierstrass solid immersion lens by an axisymmetric Bessel-modulated Gaussian beam*, Optica Applicata **43**(2), 2013: 247-259. https://doi.org/10.5277/oa130205
[10] ZHANG H., LI J., CHEN Y., *Focusing properties of power order space-variant phase modulate Bessel –Gaussian vortex beam*, Optik **249**, 2022: 168235. https://doi.org/10.1016/j.ijleo.2021.168235
[11] YE F., ZOU J., DENG D., *The effect of the spin angular momentum on the tight-focusing vortex hollow Gaussian beams*, Annalen der Physik **532**(4), 2020: 1900548. https://doi.org/10.1002/andp.201900548
[12] LIU H., ZHU Y., LIU J., WANG Y., DOU J., LI B., HU Y., *Focusing and tight-focusing properties of radially polarized Bessel-Gaussian power-exponent-phase vortex beams*, Optics Express **33**(1), 2025: 1069-1079. https://doi.org/10.1364/OE.544791
[13] WANG G., MIAO Y., LI Y., SHAN X., GAO X., *Experimental and theoretical study of linearly polarized Lorentz–Gauss beams with heterogeneous distribution*, Chinese Optics Letters **19**(2), 2021: 022602. https://doi.org/10.1364/COL.19.022602
[14] GENEVET P., YU N., AIETA F., LIN J., KATS M.A., BLANCHARD R., SCULLY M.O., GABURRO Z., CAPASSO F., *Ultra-thin plasmonic optical vortex plate based on phase discontinuities*, Applied Physics Letters **100**(1), 2012: 013101. https://doi.org/10.1063/1.3673334
[15] ZSCHOCKE S., KLIONER S.A., *On the efficient computation of the quadrupole light deflection*, Classical and Quantum Gravity **28**(1), 2011: 015009. https://doi.org/10.1088/0264-9381/28/1/015009
[16] CHAKRABORTY S., SEN A.K., *Trajectory of light ray slightly above the equatorial plane in Kerr geometry and its deflection*, Canadian Journal of Physics **95**(12), 2017: 1307-1312. https://doi.org/10.1139/cjp-2017-0168
[17] GARIEPY G., LEACH J., KIM K.T., HAMMOND T.J., FRUMKER E., BOYD R.W., CORKUM P.B., *Creating high-harmonic beams with controlled orbital angular momentum*, Physical Review Letters **113**(15), 2014: 153901. https://doi.org/10.1103/PhysRevLett.113.153901
[18] CHOPOROVA YU.YU., KNYAZEV B.A., OSINTSEVA N.D., PAVELYEV V.S., VOLODKIN B.O., *Terahertz Bessel beams with orbital angular momentum: Diffraction and interference*, EPJ Web of Conferences **149**, 2017: 05003. https://doi.org/10.1051/epjconf/201714905003
[19] PEREZHOGIN I.A., GRIGORIEV K.S., POTRAVKIN N.N., CHEREPETSKAYA E.B., MAKAROV V.A., *Transfer efficiency of angular momentum in sum-frequency generation and control of its spin and orbital parts by varying polarization and frequency of fundamental beams*, Laser Physics Letters **14**(8), 2017: 085401. https://doi.org/10.1088/1612-202X/aa77a3
[20] KAMALIA S.M., ARBABI E., ARBABI A., FARAON A., *A review of dielectric optical metasurfaces for wavefront control*, Nanophotonics **7**(6), 2018: 1041-1068. https://doi.org/10.1515/nanoph-2017-0129
[21] HE P., LI W., AN C., SUN X., YUAN W., YU Y., *Sub-diffraction-limit light sheet enabled by a super -oscillatory lens with an enlarged field of view and depth of focus*, Optics Letters **47**(13), 2022: 3267-3270. https://doi.org/10.1364/OL.461730
[22] DIAO J., YUAN W., YU Y., ZHU Y., WU Y., *Controllable design of super-oscillatory planar lenses for sub-diffraction-limit optical needles*, Optics Express **24**(3), 2016: 1924-1933. https://doi.org/10.1364/OE.24.001924

[23] ZHAO X., MA L., LIANG C., CAI Y., LI X., LIU X., *Sub-diffraction-limit realization and micro-displacement measurements via complex Gaussian-correlated beam*, Journal of Quantitative Spectroscopy and Radiative Transfer **258**, 2021: 107397. https://doi.org/10.1016/j.jqsrt.2020.107397

[24] CHEN Y., LI J., ZHANG H., XU Y., GAO X., *Focusing and propagation properties of Bessel–Gaussian beam with a power-order mixing helical–conical phase wavefront*, Applied Optics **60**(4), 2021: 929-934. https://doi.org/10.1364/AO.414356

[25] WOLF E., *Electromagnetic diffraction in optical systems. I. An integral representation of the image field*, Proceedings of the Royal Society of London. A. Mathematical and Physical Sciences **253**(1274), 1959: 349-357. https://doi.org/10.1098/rspa.1959.0199

[26] RICHARDS B., WOLF E., *Electromagnetic diffraction in optical systems. II. Structure of the image field in an aplanatic system*, Proceedings of the Royal Society of London. A. Mathematical and Physical Sciences **253**(1274), 1959: 358-379. https://doi.org/10.1098/rspa.1959.0200

Received May 14, 2025
in revised form July 28, 2025